LOAN DOCUMENT

AD-A237 423

DTIC ACCESSION NUMBER

LEVEL

INVENTORY

1

WL-TR-91-4041

DOCUMENT IDENTIFICATION

MAY 1991

DISTRIBUTION STATEMENT A

Approved for public release;
Distribution Unlimited

DISTRIBUTION STATEMENT

HANDLE WITH CARE

ACCESSION FOR
NTIS   GRAAI
DTIC   TRAC
UNANNOUNCED
JUSTIFICATION

BY
DISTRIBUTION/
AVAILABILITY CODES

DISTRIBUTION	AVAILABILITY AND/OR SPECIAL

A-1

DISTRIBUTION STAMP

QUALITY INSPECTED 1

DTIC
S ELECTE
E JUN 2 7 1991
D

DATE ACCESSIONED

DATE RETURNED

91-02821

91 6 19 231

DATE RECEIVED IN DTIC

REGISTERED OR CERTIFIED NUMBER

DTIC FORM 70A
JUN 90

DOCUMENT PROCESSING SHEET

PREVIOUS EDITIONS MAY BE USED UNTIL
STOCK IS EXHAUSTED.

LOAN DOCUMENT

AD-A237 423

VERY HIGH TEMPERATURE FIBERS OF TiC AND TiB$_2$

Dr. Richard G. Schlecht

Lasergenics Corp.
P. O. Box 611330
San Jose CA 95161-1330

May 1991

Final Report for Period April 1988 – August 1990

REPORT DOCUMENTATION PAGE

Public reporting burden for this collection of information is estimated to average 1 hour per response, including the time for reviewing instructions, searching existing data sources, gathering and maintaining the data needed, and completing and reviewing the collection of information. Send comments regarding this burden estimate or any other aspect of this collection of information, including suggestions for reducing this burden, to Washington Headquarters Services, Directorate for Information Operations and Reports, 1215 Jefferson Davis Highway, Suite 1204, Arlington, VA 22202-4302, and to the Office of Management and Budget, Paperwork Reduction Project (0704-0188), Washington, DC 20503

1. AGENCY USE ONLY (Leave blank)	2. REPORT DATE	3. REPORT TYPE AND DATES COVERED
	May 1991	Final - 88 Apr - 90 Aug

4. TITLE AND SUBTITLE

Very High Temperature Fibers of TiC and TiB2

5. FUNDING NUMBERS
PE 65502F
PR 3005
TA 52
WU None
F33615-88-C-5478

6. AUTHOR(S)

Dr. Richard G. Schlecht

7. PERFORMING ORGANIZATION NAME(S) AND ADDRESS(ES)
Lasergenics Corp.
P.O. Box 611330
San Jose CA 95161-1330

8. PERFORMING ORGANIZATION REPORT NUMBER
None

9. SPONSORING/MONITORING AGENCY NAME(S) AND ADDRESS(ES)

Materials Directorate (Dr. Richard Schlecht, WL/MLLN)
Wright Laboratory (513) 255-9834
Wright-Patterson AFB OH 45433-6533

10. SPONSORING/MONITORING AGENCY REPORT NUMBER

WL-TR-91-4041

11. SUPPLEMENTARY NOTES

This is a Small Business Innovative Research Program, Phase I report.

12a. DISTRIBUTION/AVAILABILITY STATEMENT

Approved for public release; distribution is unlimited.

12b. DISTRIBUTION CODE

13. ABSTRACT (Maximum 200 words)

The purpose of this work is to demonstrate the value of single crystal fibers of TiC and TiB2 as fibers for strengthening elements in matrix composite materials. LaserGenics has used the laser-heated pedestal-growth technique to grow short lengths of these materials in fiber form. We were not able to reduce the oxygen content in the growth chamber to a low enough of a level that would ensure single crystal growth. The fibers grown were multicrystaline and, therefore, did not possess the hoped for strength. It is clear from these early growths that single crystal fibers of these materials can be grown. Growth in a reduced level of oxygen should be done and then fibers of significant length should be grown.

14. SUBJECT TERMS		15. NUMBER OF PAGES
Composites	Single Crystals	47
Titanium Carbide		
Titanium Diboride		16. PRICE CODE

17. SECURITY CLASSIFICATION OF REPORT	18. SECURITY CLASSIFICATION OF THIS PAGE	19. SECURITY CLASSIFICATION OF ABSTRACT	20. LIMITATION OF ABSTRACT
Unclassified	Unclassified	Unclassified	UL

GENERAL INSTRUCTIONS FOR COMPLETING SF 298

The Report Documentation Page (RDP) is used in announcing and cataloging reports. It is important that this information be consistent with the rest of the report, particularly the cover and title page. Instructions for filling in each block of the form follow. It is important to **stay within the lines to meet optical scanning requirements.**

Block 1. Agency Use Only (Leave Blank)

Block 2. Report Date. Full publication date including day, month, and year, if available (e.g. 1 Jan 88). Must cite at least the year.

Block 3. Type of Report and Dates Covered. State whether report is interim, final, etc. If applicable, enter inclusive report dates (e.g. 10 Jun 87 - 30 Jun 88).

Block 4. Title and Subtitle. A title is taken from the part of the report that provides the most meaningful and complete information. When a report is prepared in more than one volume, repeat the primary title, add volume number, and include subtitle for the specific volume. On classified documents enter the title classification in parentheses.

Block 5. Funding Numbers. To include contract and grant numbers; may include program element number(s), project number(s), task number(s), and work unit number(s). Use the following labels:

C	- Contract	PR	- Project
G	- Grant	TA	- Task
PE	- Program Element	WU	- Work Unit Accession No.

Block 6. Author(s). Name(s) of person(s) responsible for writing the report, performing the research, or credited with the content of the report. If editor or compiler, this should follow the name(s).

Block 7. Performing Organization Name(s) and Address(es). Self-explanatory.

Block 8. Performing Organization Report Number. Enter the unique alphanumeric report number(s) assigned by the organization performing the report.

Block 9. Sponsoring/Monitoring Agency Names(s) and Address(es). Self-explanatory.

Block 10. Sponsoring/Monitoring Agency. Report Number. (If known)

Block 11. Supplementary Notes. Enter information not included elsewhere such as: Prepared in cooperation with...; Trans. of ...; To be published in .... When a report is revised, include a statement whether the new report supersedes or supplements the older report.

Block 12a. Distribution/Availablity Statement. Denote public availability or limitation. Cite any availability to the public. Enter additional limitations or special markings in all capitals (e.g. NOFORN, REL, ITAR)

DOD	- See DoDD 5230.24, "Distribution Statements on Technical Documents."
DOE	- See authorities
NASA	- See Handbook NHB 2200.2.
NTIS	- Leave blank.

Block 12b. Distribution Code.

DOD	- DOD - Leave blank
DOE	- DOE - Enter DOE distribution categories from the Standard Distribution for Unclassified Scientific and Technical Reports
NASA	- NASA - Leave blank
NTIS	- NTIS - Leave blank.

Block 13. Abstract. Include a brief (Maximum 200 words) factual summary of the most significant information contained in the report.

Block 14. Subject Terms. Keywords or phrases identifying major subjects in the report.

Block 15. Number of Pages. Enter the total number of pages.

Block 16. Price Code. Enter appropriate price code (NTIS only).

Blocks 17. - 19. Security Classifications. Self-explanatory. Enter U.S. Security Classification in accordance with U.S. Security Regulations (i.e., UNCLASSIFIED). If form contains classified information, stamp classification on the top and bottom of the page.
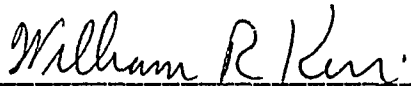
Block 20. Limitation of Abstract. This block must be completed to assign a limitation to the abstract. Enter either UL (unlimited) or SAR (same as report). An entry in this block is necessary if the abstract is to be limited. If blank, the abstract is assumed to be unlimited.
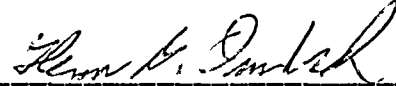
This technical report has been reviewed and is approved for publication.

WILLIAM R. KERR
Metallurgist
Materials Behavior Branch
Metals and Ceramics Division

GLENN G. ORMBREK
Technical Area Manager, Actg.
Materials Behavior Branch
Metals and Ceramics Division

FOR THE COMMANDER

ALLAN W. GUNDERSON
Actg. Branch Chief
Materials Behavior Branch
Metals and Ceramics Division

TABLE OF CONTENTS

PROJECT SUMMARY

The purpose of this work is to demonstrate the value of single crystal fibers of TiC and TiB$_2$ as fibers for strengthening elements in matrix composite materials. Single crystal fibers have the capability for significantly strengthening composite materials for high temperature applications. If fibers of high quality can be grown of sufficient length, they could have an important impact on the development of new high performance jet and rocket engine components as well as other airframe components that experience high temperature environments.

LaserGenics has used the laser-heated pedestal-growth technique to grow short lengths of these materials in fiber form. Both TiC and TiB$_2$ are quite reactive in air and some care must be exercised to reduce the oxygen content in the growth atmosphere. We were not able to reduce the oxygen content in the growth chamber to a low enough of a level that would ensure single crystal growth. The fibers grown were multicrystaline and, therefore, did not possess the hoped for strength. By making improvements in the growth chamber so that the atmosphere could be more precisely controlled, we feel, based on our results, that single crystal fibers of these materials could indeed be grown and incorporated into matrix composite materials.

It is clear from these early growths that single crystal fibers of these materials can be grown. Growth in a reduced level of oxygen should be done and then fibers of significant length should be grown. These fibers should be tested in matrix composite materials at elevated temperatures to see if they could result in materials that could be used in the critical components of the new generation jet and rocket engines. If successful, this could result in higher operating temperatures for these engines and thereby improved efficiency. This could also result in increased reliability for these systems.

Section 1

INTRODUCTION

Aerospace propulsion systems have become highly sophisticated and they require materials that are capable of withstanding extremely demanding environments. Composite materials utilizing high strength fibers are very attractive materials for meeting the demands of these extreme environments. To date these materials have not met their potential in strength and high temperature capabilities. Fibers produced by sintering the solid have not produced the strengths hoped for. The highest strengths observed have been with single crystal whiskers. The observed strengths have been near the theoretical limits, between 3 and 17 % of the elastic modulus. Although whiskers have demonstrated high tensile strengths, they have not been widely used because they are difficult to grow and can not be grown in sufficient lengths. As ceramic fibers are not able to achieve strengths approaching the theoretical limit, it would seem that if single crystal fibers of adequate length could be grown, these fibers could have wide use in specialized composite materials where high tensile strength, high thermal conductivity, light weight and high melting points are required. We have investigated the growth of fibers of TiB_2 and TiC.

From the observed strength of single crystal fibers, Brenner[1] has calculated that at temperatures above 650 °C a composite containing 50% by volume of sapphire fibers is potentially much stronger than any of the present-day superalloys (see Figure 1). If it is true as is assumed that the fibers in a composite carry almost all of the applied load, the most important factor limiting the strength of composites is the strength of the fibers. Therefore, the selection of the fiber is crucial to determining the strength of any composite material

Some of the factors that effect the strength of single crystal fibers other than the crystal composition are the crystal quality (impurities, dislocations, voids, etc.), surface quality and the fiber diameter. Clearly, the lower the density of dislocations, cracks, voids and impurities the stronger the fiber will be. As the surface of the fiber plays such a large part in determining the strength of small diameter fibers it is no surprise that the strength of a single crystal fiber is strongly dependent on the fiber diameter. Therefore to optimize the strength of a single crystal fiber, we must be able to grow the fibers in small diameters with high purity and few defects.

As we mentioned above, the growth of whiskers has been studied for many years and yet it is still not possible to grow the lengths required and control the growth as one would like. Therefore, many other techniques have been studied recently to grow long lengths of single crystal fibers with controlled diameters. As early as 1922, Von Gomperz[2] developed a technique for the continuous growth of metal fiber crystals from their melts. In 1960, Gaule and Pastore[3] studied the role of surface tension in pulling single crystals of controlled dimensions and discussed the concept of guided melts and its application to the growth of Ge single crystal filaments. In 1967, LaBelle and Mlavsky[4] reported on the growth of sapphire filaments using a modified Czochralski puller and rf heating. Fibers with diameters in the range of 50-500µm were grown at rates of up to 150 mm/min. These c-axis fibers, which were probably grown dendritically, had an average tensile strength of 300,000 lb/in^2. Their strength was much higher than bulk crystals prepared by the flame fusion technique which had tensile strengths in the 72,000-102,000 lb/in^2 range.[5] Vapor grown sapphire whiskers, however, had much higher, nearly theoretical tensile strengths in the 1-2x10^6 lb/in^2 range.[6] LaBelle and Mlavsky found that when their fibers were accurately oriented along the c-axis, the external surfaces were smooth, but if the fiber axis departed slightly from this orientation the

2

external surface of the fiber reflected this in its morphology. In 1971, LaBelle and Mlavsky[7] published on the growth of sapphire fibers by the now famous die-shaped growth method known as edge-defined film-fed growth (EFG). These fibers were grown in different orientations with c-axis fibers grown at rates as high as 200mm/min. The major drawback to this approach for high temperature materials is that the die material must be able to withstand the melting point of the source material. Even in the case of sapphire, the in-diffusion of the molybdenum die material seriously adds to the impurity level of the grown fiber, thereby adversely affecting the strength of the fiber.

In 1972, Haggerty[8] reported on the development of a four beam laser-heated float-zone system specifically designed for the preparation of single crystal fibers. He grew fibers of Al_2O_3, Y_2O_3, TiC and TiB_2 for evaluation, principally to study their mechanical properties. The idea of using laser heating for crystal growth, however, originated with Gasson and Cockayne[9] who prepared relatively large single crystal boules of high melting oxides such as Al_2O_3, Y_2O_3, $MgAl_2O_4$ and Nd_2O_3 by this method. Haggerty grew fibers oriented in several directions, explored several growth atmospheres including air, Ar, Cl_2, H_2 and CH_3 alone and in various combinations, growth direction and rate, beam energy density and angle, and radiation shielding. These early fiber growth activities[7,8] were directed mainly toward fibers for high-strength lightweight composites. In the mid-1970's Burris and Stone[10,11] applied a technique similar to Haggerty's to investigate small diameter fibers for laser applications. Small diameter fibers of Nd:YAG and Nd:Y_2O_3 were grown.

LaserGenics Corporation has recently obtained the exclusive rights to the three patents held by Stanford University on single crystal fiber growth processes using the laser-heated pedestal-growth (LHPG) technique. We are

developing these processes in order to obtain high quality single crystal fibers of several meter lengths. Single crystal fibers of sapphire, YAG, ruby, $LiNbO_3$, TiC, TiB_2 and a whole host of other materials have already been successfully grown on a research basis.

An important aspect of this technique is that the purity of the fiber is completly dictated by the purity of the starting material as nothing but the controlling atmosphere comes in contact with the molten zone of the source rod. The LHPG technique is an excellent method to grow single crystal fibers with very high melting points. It is likely that for many such high melting point materials no other technique will be able to grow similarly good quality single crystal fibers.

The primary objective of our program was to investigate the growth of single crystal fibers of TiB_2 and TiC for potential use in very high temperature composite materials for advanced gas trubine engines and transatmospheric flight vehicles. We have:

1) grow several different diameters of single crystal fibers of TiB_2 and TiC;

2) measure the tensile strength of these fibers; and

3) develop a program for optimizing the growth and dimensions of the fibers to meet the requirements of composite materials for Air Force applications.

The successful completion of this research would result in single crystal fibers that would have widespread application in composite materials for high strength and high temperature applications.

In section 2 we discuss the physics of strong materials. We describe what are the important parameters which determine the strength of any solid material In section 3 we discuss the effects of cracks and dislocations on the strength of strong materials In section 4 we discuss fiber reinforced

4

solids and why they result in substantial strengthening of solids. In section 5 we discribe the laser-heated pedestal-growth technique and why this method is unique for the growth of strong single crystal fibers. Finally, in section 6 we present the results of our experimentation.

Section 2

STRONG MATERIALS

The purpose of this section is to determine what makes a strong material. If we know what it is that makes a strong material, we may be able to develop materials that are near their theoretical limit for strength.

One would expect that a perfect crystal would be the strongest solid. Therefore calculations on these systems are of interest to indicate the limits one might expect for materials. To make such model calculations, it is necessary to select an interatomic potential that is accurate even when the crystal is distorted. Polanyi[12] and Orowan[13] developed a simple theory that gives a reasonable estimate of the tensile stress of a solid. They assume that the stress in pulling apart any solid varies with displacement as a sine function. This is given in Equation 2.1 as:

$$\sigma = K \sin (\pi/a)(x - a_0) \qquad\qquad 2.1$$

The constant K can be found by relating the slope of the stress displacement curve at equilibrium to Young's modulus. This gives:

$$K = (E/\pi)(a/a_0) \qquad\qquad 2.2$$

where a is a measure of how far the interatomic planes must be displaced before fracture occurs.

Polyani[12] and Orowan[13] relate the integral of the stress from equilibrium to fracture to the surface energy, g, of the two surfaces formed Thus:

$$a - \pi g/K. \qquad\qquad 2.3$$

Therefore, since a is of the same order of magnitude as a_0, we have that:

$$g = Ea_0/\pi^2 \approx Ea_0/10 \qquad\qquad 2.4$$

From 2.1 we can also calculate the maximum theoretical cleavage stress to be:

$$\sigma_{max} = K = \sqrt{(Eg/a_0)} \qquad\qquad 2.5$$

Therefore, strong materials will have large values of the Young's modulus and the surface energy and small values of the interplanar spacing. Clearly, this is an isotropic theory that does not take into account the planar nature of crystalline solids. However, the theory has been found to give the right order of magnitude in most cases and generally overestimates the strength by a factor of two. Table I are the results calculated for the cleavage stress for several materials using this theory. It is interesting to note from this table that sapphire is one of the strongest materials in the table with a high melting point.

In order to obtain a more exact description of the strength of materials, we must have a more accurate description of the inter-atomic forces that act in the material. de Boar[14] was the first to apply the Morse potential, given by Equation 2.6, to the strength of materials. If the constants of the potential can be determined from spectroscopic data, results closer to the measured values can be achieved.

$$U - U_0[\exp(-2a(r-r_0)) - 2\exp(-a(r-r_0))] \qquad\qquad 2.6$$

TABLE I

Material	Direction	E (GPa)	Surface Energy (mJm^{-2})	S_{max} (GPa)
Silver	⟨111⟩	121	1130	24
Silver	⟨100⟩	44	1130	16
Gold	⟨111⟩	110	1350	27
Copper	⟨111⟩	192	1650	39
Copper	⟨100⟩	67	1650	25
Nickel	⟨100⟩	138	1730	37
Tungsten	⟨100⟩	390	3000	61
a-Iron	⟨111⟩	260	2000	46
a-Iron	⟨100⟩	132	2000	30
Zinc	⟨0001⟩	35	100	3.8
Sodium	⟨100⟩	1.46	228	0.9
Sodium	⟨111⟩	10.5	228	2.5
Graphite	⟨0001⟩	10	70	1.4
Silicon	⟨111⟩	188	1200	32
Diamond	⟨111⟩	1210	5400	205
Silica Glass		73	560	16.0
Sodium Chloride	⟨100⟩	44	250	6.3
Magnesium Oxide	⟨100⟩	245	1200	37
Aluminium Oxide	⟨0001⟩	460	1000	46

Potential functions other than the Morse potential have been used to calculate the strength of solids. Zwicky[15] calculated the strength of alkali halides using for the potential energy between a pair of ions the expression.

$$\emptyset = \pm e^2/r + A/r^9. \tag{2.7}$$

The Born-Mayer model, with and without Poisson contraction, has also been used for ionic crystals. These calculations have been reviewed by Macmillan.[16] Macmillan and Kelly[17] have investigated the use of the Lennard-Jones potential for van der Waals bonding. This potential is given by.

$$\emptyset(r) = 2U[-(r_0/r)^6 + (1/2)(r_0/r)^{12}] \qquad\qquad 2.8$$

These more exact methods for calculating the tensile or cleavage stress of ionic solids typically yield values that are about half those obtained from Orowan's estimate. These techniques have also been applied to metals but because of the much more complex ion-ion interactions in these materials, these calculations are more approximate. We will not discuss these calculations as we are concerned primarily with ionic solids and because the strengths of metals, particularly at elevated temperatures, does not approach those of ionic solids.

In a similar fashion to the way we calculated the tensile stress, we can calculate the shear stress. Frenkel[18] has made such a calculation using very simple assumptions. If you consider two neighboring planes of ions in a crystal which are separated by a distance h and have a repeat distance of b in the direction of the shear, and assume that the planes remain undistorted during the application of the shear stress τ, we can then assume that the shear stress has the form:

$$\tau - k \sin(2\pi x/b) \qquad\qquad 2.9$$

For small shear displacements x, we have that h dτ/dx is equal to the shear modulus, G, so that k is equal to Gb/2πh. Then the maximum value of the shear stress, τ_{max}, occurs at x = b/4, and is given by:

$$\tau_{max} - Gb/2\pi h. \qquad\qquad 2.10$$

A more complete calculation of the maximum shear stress has been made

by Mackenzie.[19] The variation of the potential energy per unit area as a function of the displacement, x, is given in the Frenkel theory by:

$$U(x) = (Gb^2/4\pi^2h)(1 - \cos(2\pi x/b))$$

2.11

This is equivalent to considering only the first term in a Fourier series for the potential energy. Mackenzie determined how to take higher order terms into account. He calculated the coefficients of the higher order terms for several crystal structures from general arguments. Values of the theoretical shear strength calculated by Mackenzie's method for several different crystals is given in Table II.

In Table II the theoretical shear strength of sapphire is given. The slip geometry is shown in Figure 2.1. Taking account of the fact that the oxygen ions are not close-packed, the value of τ_{max}/G is 0.115. This will only be a rough estimate of the shear strength.

A number of calculations have also been done using the same techniques we have already described to calculate the tensile strength. The Born-Mayer model was used by Tyson[20], Macmillan[21] and Macmillan and Kelly.[22,23] to investigate solid argon and sodium chloride. Tyson also investigated the application of the Lennard-Jones potential to determine the maximum shear stress. Kobayashi, Maeda and Takeuchi[24] used a modified Lennard-Jones potential to study crystalline copper and zirconium. Huang, Milstein and Baldwin[25] and Basinski, et al.[26] have studied the ideal shear strength of metals using a generalized Morse potential.

For our application, one of the most important considerations is the performance of the materials at high temperature. Therefore the temperature dependence of the material strength will be important to determine. From Equation 2 10, we can see that the temperature dependence of the shear stress

TABLE II

Material	Elastic Constant G' (GPa)	τ_{max}/G'	τ_{max} (GPa)
Cu (at 10°K)	33.2	0.039	1.29
Cu	30.8	0.039	1.2
Au	19.0	0.039	0.74
Ag	19.7	0.039	0.77
Co	84	0.039	3.49
Al	23	0.039	0.9
Al	23	0.114	2.62
Ni	62	0.039	2.4
Ni	62	0.114	7.1
Si	57	0.24	13.7
Fe	60	0.11	6.6
W	150	0.11	16.5
Al_2O_3	147	0.115	16.9
Zn	38	0.034	2.3
Graphite	2.3	0.05	11.5×10^{-2}
NaCl	18	0.159	2.9

is the same as the temperature dependence of the shear modulus and is determined by the temperature dependence of the interatomic spacing which is not strongly temperature dependent. However, the tensile strength is not so simply related to the temperature because of the uncertainty of how the
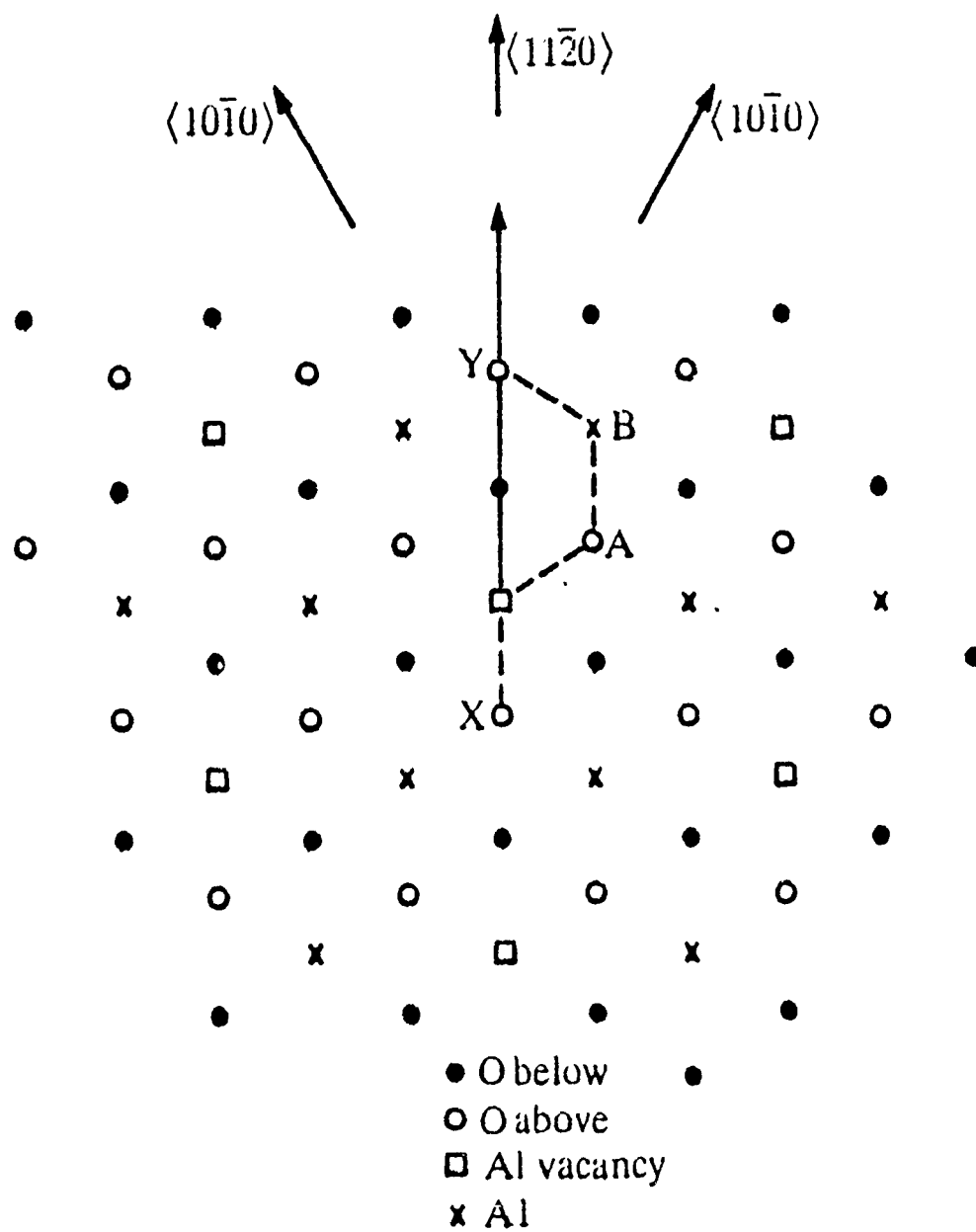
Figure 2.1. The slip plane of sapphire (Al_2O_3) where the distance XY represents one complete unit of slip

surface energy is related to the temperature. Nishioka and Lee[27] used the Einstein model where each atom is assumed to perform harmonic motion with a frequency determined from an interatomic potential that was calculated in a self consistent way. However, the experiments of Milstein[28] and Parinello and Rahman[29] on nickel showed a much stronger dependence on temperature than that calculated by Nishioka and Lee. Gilyarov[30] made similar calculations on a simple cubic lattice that showed a more sensitive temperature dependence.

As we will see in the next section, the practical limits on the strength of solids is determined by defects within or on the surface of the solid. At a finite temperature, a crystal can fail due to the propagation of a crack or dislocation. Frank[31] and Hirth[32] have shown that if a dislocation of radius R is formed in a crystal under a shear stress τ, the energy of the crystal is increased by U, where U is given by:

$$U = \pi R^2(g-\tau b) + (1/2)Gb^2 R\ln(R/r_0) \quad 2.12$$

Taking the derivative of U with respect to R and setting to 0 we obtain a value for the critical radius of the dislocation given by:

$$R_c(1-g/\tau b) = (Gb/4\pi\tau)(\ln(R_c/r_0)+1) \quad\quad 2.13$$

The critical energy is then given by:

$$U_c = R_c(Gb^2/4)(\ln(R_c/r_0) - 1) \quad\quad 2.14$$

If the dislocation is formed on the surface of the crystal, the critical energy is one half of the bulk value as only one surface is involved in the dislocation rather than two. However, the critical radius is the same in the two

cases. Therefore, it is easier to thermally reach this critical energy for surface defects than for bulk defects. A loop of radius smaller than R_c will contract while a loop of radius larger will grow. Therefore, U_c represents an activation energy. Then, if g is small compared to Gb, a partial dislocation will be nucleated and b must be set to the partial reciprocal lattice vector b_p. Then $(1-(g/\tau b)) \approx 1$. For sapphire $Gb/g \approx 40$ so that this is a good approximation. To estimate the temperature dependence of the ideal shear strength, we suppose that thermal fluctuations can supply up to 50kT in energy at any temperature. Knowing r_0 and b from the crystal structure and the value of G for the material, we can determine the temperature dependence. For sapphire we have that $b_p = 0.159$ nm, $r_0 \approx 0.204$ nm and G = 147 GPa. From this we calculate a critical radius, R_c, at 300°K of 0.75 nm and a G/τ of 25.8. At 2000°K, we find that R_c is approximately 1.5 nm and G/τ is about 39.6. Therefore the shear strength is reduced by approximately 35% between 300°K and 2000°K.

To determine the tensile strength as a function of the temperature, we consider the introduction of a penney-shaped crack of radius R into the solid so that the crack is oriented perpendicular to the tensile axis. The Young's modulus will vary with the applied stress as:

$$E(\sigma) = E(1 - \sigma^2/\sigma_{max}^2) \qquad 2.15$$

where E is the conventional Young's modulus. Then the crack will release strain energy within a spherical volume about the crack given by:

$$U = (4\pi R^3/3)(\sigma^2/2E)(1 - \sigma^2/\sigma_{max}^2)^{-1/2} + 4\pi R^2 g \qquad 2.16$$

Determining the critical radius by setting the derivative of U with respect to R equal to zero. we have that:

$$R_c = (4Eg/\sigma^2)(1 - \sigma^2/\sigma_{max}^2)^{1/2} \qquad 2.17$$

Substituting this expression into 2.16, we have that:

$$U_c = (64\pi E^2 g^3/3\sigma^4)(1 - \sigma/\sigma_{max}^2) \qquad 2.18$$

We again set U_c equal to 50kT in order to determine the temperature dependence of the tensile strength. For sapphire we set E = 460 GPa, σ_{max} = 46 GPa and g = 1 J/m^2. Then, for T = 300°K we find that σ = 45 GPa so that the tensile strength is reduced by approximately 2%. At T = 2000°K we find that σ = 40 GPa or that the tensile strength declines by 11% from its value at 300°K. The critical radius increases from its value of 0.19 nm at 300°K to 0.57 nm at 2000°K.

We can now draw some conclusions from our earlier discussions. Equation 2.5 shows that a large breaking strength requires a large Young's modulus, a large surface energy and a small interatomic spacing. A strong solid will have a large value for both σ_{max} and τ_{max}. This generally occurs in solids with directional bonds. Such bonds are found in covalently bound materials or in materials with strongly polarized ionic bonds. Covalent bonds are strongest when they are composed of small atoms linked by short bonds resulting in a large number of bonds per unit volume. The valency of the atoms must be at least three in order to insure a three dimensional lattice. For an ionic crystal, the elastic modulus increases directly as the product of the valencies of the

ions and inversely as the fourth power of the interatomic distance.[33] Therefore, strong ionic solids contain small ions with high valence. These ions are highly polarizable so that strong ionic crystals contain strongly polarized bonds. Thus, we may say that for strong materials we must have a high density three-dimensional network of strong directional bonds. The elements that can possess these properties are beryllium, boron, carbon, nitrogen, oxygen, aluminum and silicon. The strongest materials always contain one or more of these elements.

Some important consequences of this definition of a strong solid must follow. Small atoms insure the presence of the lighter elements and highly directional bonds imply non-close-packed crystal structures resulting in low densities. A large elastic modulus means a large binding energy which implies a high melting point and a low coefficient of thermal expansion. Restating, the strongest materials will have a high elastic modulus, a low density, a high melting point and a low thermal expansion coefficient.

Unfortunately, these large strengths are rarely achieved in practice. Solids normally contain many imperfections which cause them to break at stresses much lower than the ideal strength. The fracture mechanism will be either through cleavage or dislocation. These mechanisms will generally determine the strength of a material. In the next section we will discuss these processes which in a large way determine the strength of solids.

Section 3

CRACKS AND DISLOCATIONS

A crack is a flaw at the surface or in the interior of a solid where a high stress is concentrated. At the tip of the crack the stress may reach levels close to the tensile limit of the material. Dislocations occur when crystal planes glide over one another. These can occur at shear stresses much less than the theoretical limit. This is also referred to as plastic flow. We will first consider the case of cracks in solids.

The determination of the stresses in a solid with a crack in the interior is a very difficult problem. We will consider a very simple case which has been worked out by Inglis[34] and Kolosoff.[35] This determination can also be found in the book by Timoshenko and Goodier.[36] This example gives a clear idea of the stresses caused by such cracks.

We consider an elliptical hole which passes through an infinite and thin plate. The equation of the hole centered at the origin is given by:

$$x^2/a^2 + y^2/b^2 = 1 \qquad\qquad 3.1$$

The radius of curvature at the end of the major axis is equal to $b^2/a = \beta$ and at the minor axis end is a^2/b. We also define the parameter $e = b/a$ in terms of which we can write the radius of curvature β at the end of the major axis as $e^2 a$ We can transform the ellipse so that it has unit radius of curvature at the end of the major axis and so that the origin is at this point. The equation of the ellipse then becomes:

$$[(x + a/\beta)/(a/\beta)]^2 + [y'/\sqrt{(a/\beta)}]^2 = 1 \qquad\qquad 3.2$$

Using this form we examine the case of a thin sharp crack which corresponds to $ß/a \rightarrow 0$. In this limit we obtain for the form of the crack near the tip:

$$y'^2 = -2x'$$
3.3

If we now apply a uniform tensile stress parallel to the minor axis, the tensile stress in this direction at the tip of the crack is given by:

$$\sigma_{max} = \sigma[1+(2a/b)] = \sigma[1 + \sqrt{(a/ß)}]$$
3.4

This is the maximum stress present. At the minor axis there is a compressive stress present of magnitude $\sigma_{min} = -\sigma$. In the direction along the major axis, the stress parallel to the applied stress rapidly falls from the value given by 3.4 to the value σ. The stress perpendicular to the applied stress rises from zero at the crack surface to a maximum value at a distance b^2/a from the surface and then falls back to zero. Its maximum value is approximately one fifth of 3.4. Along the minor axis, the tensile stress perpendicular to this axis changes in a distance of approximately $ß$ from $-\sigma$ to a small positive tensile stress and then gradually to zero. The tensile stress parallel to the minor axis is zero at the crack surface and gradually rises to the value σ. In Figure 3.1 the tensile stress parallel and perpendicular to the major axis as a function of the distance from the origin is plotted. Schijve[37] has calculated the shear stress in terms of polar coordinates far many values of a/b around the crack tip. He has given many interesting graphs of his results in his paper.

The results just given apply to isotropic materials. Many materials, and in particular most fibers, are orthotropic; that is materials that possess three planes of symmetry that are perpendicular to one another. Bishop[38]
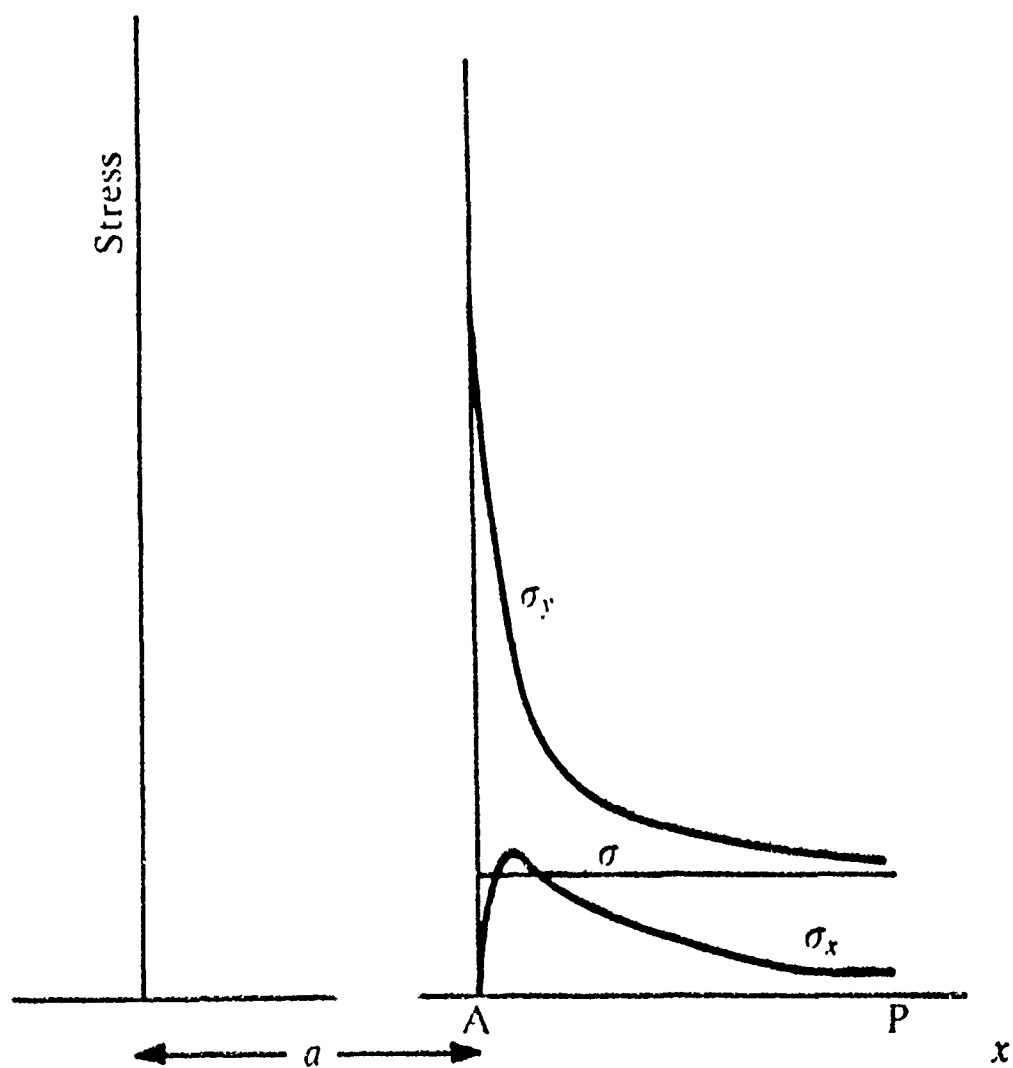
Figure 3 1 Variation of σ_x and σ_y along major axis of crack of length a

investigated the stress around an elliptical hole oriented perpendicular to the fiber axis. He considered a carbon fiber reinforced composite with the stress parallel to the fiber axis. Bishop determined that the stresses scale as $\sigma\sqrt{a/\beta}$. The parallel tensile stress maximum occurs at the end of the major axis and is given by:

$$\sigma_{y\,max}/\sigma = (\mu_1 + \mu_2)/(\mu_1\mu_2) + \epsilon \qquad 3.5$$

$$\text{where:} \quad \mu_1^2 = \alpha E_{xx}[1 + (1-1/(\alpha^2 E_{xx} E_{yy}))^{1/2}]; \qquad 3.6$$

$$\mu_2^2 = \alpha E_{xx}[1 - (1-1/(\alpha^2 E_{xx} E_{yy}))^{1/2}]; \qquad 3.7$$

$$\alpha = (1/2G_{xy}) - (v_{yx}/E_{yy}) = (1/G_{xy}) - (v_{xy}/E_{xx}); \text{ and} \qquad 3.8$$

$$\epsilon = \sqrt{\beta/a} \qquad 3.9$$

where E_{ii} are the anisotropic Young's modulii, G_{ii} are the anisotropic shear modulii and v_{ii} are the anisotropic Poisson's ratios.

The perpendicular compressive stress maximum occurs at the end of the minor axis and is given by:

$$(-\sigma_{x\,max})/\sigma = \mu_1\mu_2 \qquad 3.10$$

From these expressions we can determine the stresses that exist for a crack by letting ϵ go to zero. For the parallel tensile stress maximum we get that:

$$\sigma_{ymax}/\sigma = 1 + \sqrt{(a/\beta)}(2(\sqrt{(E_{yy}/E_{xx})} - v_{yx}) + E_{yy}/G_{xy}) = (\sigma\sqrt{(a/\beta)})^2/\sigma_{xmax}$$

<div align="right">3.11</div>

We can extend the analysis we have given for the stress caused by a cavity in a solid to the surface of the solid by considering a notch at the surface. This has been done by Inglis[34] and by Bishop.[38] Inglis has shown that the stresses at the end of a cavity or a notch depends almost entirely on the length of the cavity. It does not make too much difference what the shape of the cavity is, only that the tip can be approximated by an ellipse. A notch is formed by cutting the plate we considered earlier along the minor axis. The stresses in a plate with this elliptical notch will have the same maximum tensile stress at the end of the notch as the cavity, for an isotropic material we found this to be $\sigma_{ymax} = \sigma(1+2\sqrt{(a/\beta)})$.

Equations 3.10 and 3.11 can be used to calculate the concentrated stress around the end of a hole or a notch for an isotropic or orthotropic material, respectively. For example, if the radius of curvature at the end of a crack of length 6 μm or notch of length 3 μm is 3 nm, the applied stress in an isotropic material will be magnified by a factor of 64. Clearly, this can lead to the attainment of fracture strength at the end of a crack or notch at relativly small applied stresses. This can than lead to material failure. Because of this stress magnification, solids usually fail due to the existence of such defects.

Griffith has developed an energy balance theory that has accounted in a large way for the discrepancy between the calculated values of the strength of ideal brittle solids and the observed values for real solids. Griffith postulated that this discrepancy was due to the existance of cracks and notches and that rupture occurrs by the spreading of these cracks and notches. Griffith found from his analysis that the tensile stress perpendicular to a crack of length c in an isotropic solid that causes the crack to propagate is:

$$\sigma = \sqrt{(2Eg/\pi c)} \qquad\qquad 3.12$$

in plane stress, and

$$\sigma = \sqrt{(2Eg)/(\pi(1-v^2)c)} \qquad\qquad 3.13$$

in plane strain. Griffith also found that the strength was not reduced by a stress parallel to the crack. He also found that for a notch of depth c, Equations 3.12 and 3.13 are valid for the two cases if each is multiplied by a constant factor 0.89. Therfore, surface defects will be very important in determining the strength of fibers.

Section 4

FIBER REINFORCED SOLIDS

In the previous sections we have seen that strong solids are sensitive to cracks. Clearly, fibers will be more useful than the bulk as an engineering material as the cracks across a fiber must be short because of the small diameter of the fiber or they will be along the fiber where they will not effect the strength of the material. Therefore a very strong solid with a high and reproducible strength can be formed by having a large number of fibers parallel to one another and imbedded in another solid. The parallel fibers will be much less susceptible to cracking than an equivalent mass of the bulk material. However, the fibers will have no strength perpendicular to the fiber axes.

The solid in which the strong fibers are imbedded is called the matrix. The matrix has several important functions when used with fibers of strong materials. First, it supplies the medium by which the load is transmitted to the fibers. Secondly, it separates the individual fibers so that a crack in one of the fibers can not propagate. Finally, it protects the surface of the fibers so that the fibers do not lose their strength by abrasion with other fibers or with another material.

We will now attempt to give some explanation of the strength of a composite from the properties of the two components which make up the material From classical elasticity theory it can be shown[39] that for a two component system the volume average of the stress components are functions of the tractions at the boundary only and the volume average of the strain components are functions of the surface displacements. Then, by determining the stresses and strains in a fiber composite, the elastic moduli can be determined for a homogeneous system An aligned composite will have five

constants if the system is orthotropic and is isotropic in the plane perpendicular to the fiber axis. Under these conditions five constants can be selected so that only one moduli appears in the strain energy function. These moduli are:

$$E_z = C_{33} - (2C_{13}^2/(C_{11} + C_{12})) \tag{4.1}$$

$$G = G_{xz} = G_{yz} = C_{44} \tag{4.2}$$

$$K_p = (C_{11} + C_{12})/2 \tag{4.3}$$

$$G_{xy} = E_x/2(1 + v_{xy}) = (C_{11} - C_{12})/2 \tag{4.4}$$

and C_{33}. The z axis is the fiber axis. E_z is Young's modulus parallel to the fiber axis and E_x perpendicular to the fiber axis. G is the shear modulus for shear parallel to the fiber axis and K_p is the strain bulk modulus for strain applied in the x-y plane with no contraction along z. Hashin[40] obtained bounds for K_p, G_{xy}, and G. Hill[41] had obtained bounds for E_z, K_p and v, the Poisson's ratio relating transverse contraction to strain parallel to the fibers. These bounds are represented by the following equations:

$$E = E_1 V_1 + E_2 V_2 + 4 V_1 V_2 (v_2 - v_1)^2 \Big/ \left[(V_2/K_{p1}) + (V_1/K_{p2}) + G_2^{-1} \right] \tag{4.5}$$

$$v = v_1 V_1 + v_2 V_2 + V_1 V_2 (v_1 - v_2)(K_{p2}^{-1} - K_{p1}^{-1}) \left[(V_2/K_{p1}) + (V_1/K_{p2}) + G_2^{-1} \right]^{-1}$$

$$\tag{4.6}$$

$$K_{xy}^{-1} = (V_1/K_{p1}) + (V_2/K_{p2}) - V_1 V_2 \left(K_{p1}^{-1} - K_{p2}^{-1} \right)^2 \Big/ \left[(V_2/K_{p1}) + (V_1/K_{p2}) + \right.$$

$$\left. G_2^{-1} \right]^{-1} \tag{4.7}$$

$$G^{-1} = V_1/G_1 + V_2/G_2 - V_1 V_2 (G_1 - G_2)^2 / \left[G_1 G_2 (G_1 (1 + V_1) + G_2 V_2) \right] \qquad 4.8$$

$$G_{xy}^{-1} = V_1/G_1 + V_2/G_2 - V_1 V_2 (G_1 - G_2)^2 / \left[G_1^2 G_2^2 \left(V_2/G_1 + V_1/G_2 + \right. \right.$$

$$\left. \left. 2/K_{p2} + G_2^{-1} \right) \right] \qquad 4.9$$

In these expressions V_1 and V_2 are the volume fractions of the two components. If $G_2 > G_1$ and $K_{p2} > K_{p1}$, these expressions give the upper bounds on the five moduli. The lower bounds are obtained by interchanging the suffixes 1 and 2. If $G_1 > G_2$ and $K_{p1} > K_{p2}$, the expressions give the lower bound. The upper bounds are obtained for this case by interchanging the suffixes 1 and 2 as before. For $G_1 = G_2$ the expressions are exact. For most practical cases $G_1 > G_2$ as the fiber is more rigid than the matrix.

The expressions for the upper and lower bounds of the axial Young's modulus and the Poisson's ratio are close together in value so that they can be used for a good approximation to the true values. Hashin[42] has reviewed the attempts that have been made to obtain good values for these moduli.

From equations 4.7 and 4.8 we see that the strain bulk modulus in the plane and the shear modulus of the composite are in large part determined by the properties of the matrix as $1/K_{p2} \gg 1/K_{p1}$ and $1/G_2 \gg 1/G_1$. The transverse shear modulus is also dominated by the shear modulus of the matrix when this is much less than that of the fibers. For a transversely isotropic composite, the transverse Young's modulus is given by:

$$E_t = 4K_{xy} G_{xy} / \left\{ K_{xy} + G_{xy} \left[1 + (4 K_{xy} v^2 / E) \right] \right\} \qquad 4.10$$

We now define the strength of the composite, σ_c, as the maximum load divided by the initial cross sectional area. We use subscripts c, f, and m to refer to the composite, fibers, and matrix, respectively. The ultimate tensile strength of the composite may be written:

$$\sigma_{uc} = \sigma_{uf} V_f \lambda_f + \sigma_{um} V_m \lambda_m \qquad \qquad 4.11$$

λ_f and λ_m are complicated expressions containing the constants used to describe the stress-strain curves of the components. If the ultimate tensile strains of both components are the same, λ_f and λ_m both equal unity and we have that:

$$\sigma_{uc} = \sigma_{uf} V_f + \sigma_{um} V_m \qquad \qquad 4.12$$

This expression gives an upper limit to the tensile strength of the composite. If the ultimate tensile strain of the fibers is much less than that of the matrix and $\sigma_{uf} V_f \gg \sigma_{um} V_m$ then 4.12 becomes:

$$\sigma_{uc} = \sigma_{uf} V_f + \sigma'_m (1 - V_f) \qquad \qquad 4.13$$

where σ'_m is the stress on the matrix at the ultimate tensile strain of the fibers. The envelope of possible strengths for the composite is shown in Figure 4.1 The strength must lie within the triangle AOB. From these expressions we see that as the volume fraction of the fibers increases, the strength of the composite will approach that of the fiber.

For a brittle matrix we have that $\epsilon_{ym} \approx \epsilon_{um}$. If we also have that $\epsilon_{uf} \gg \epsilon_{um}$,
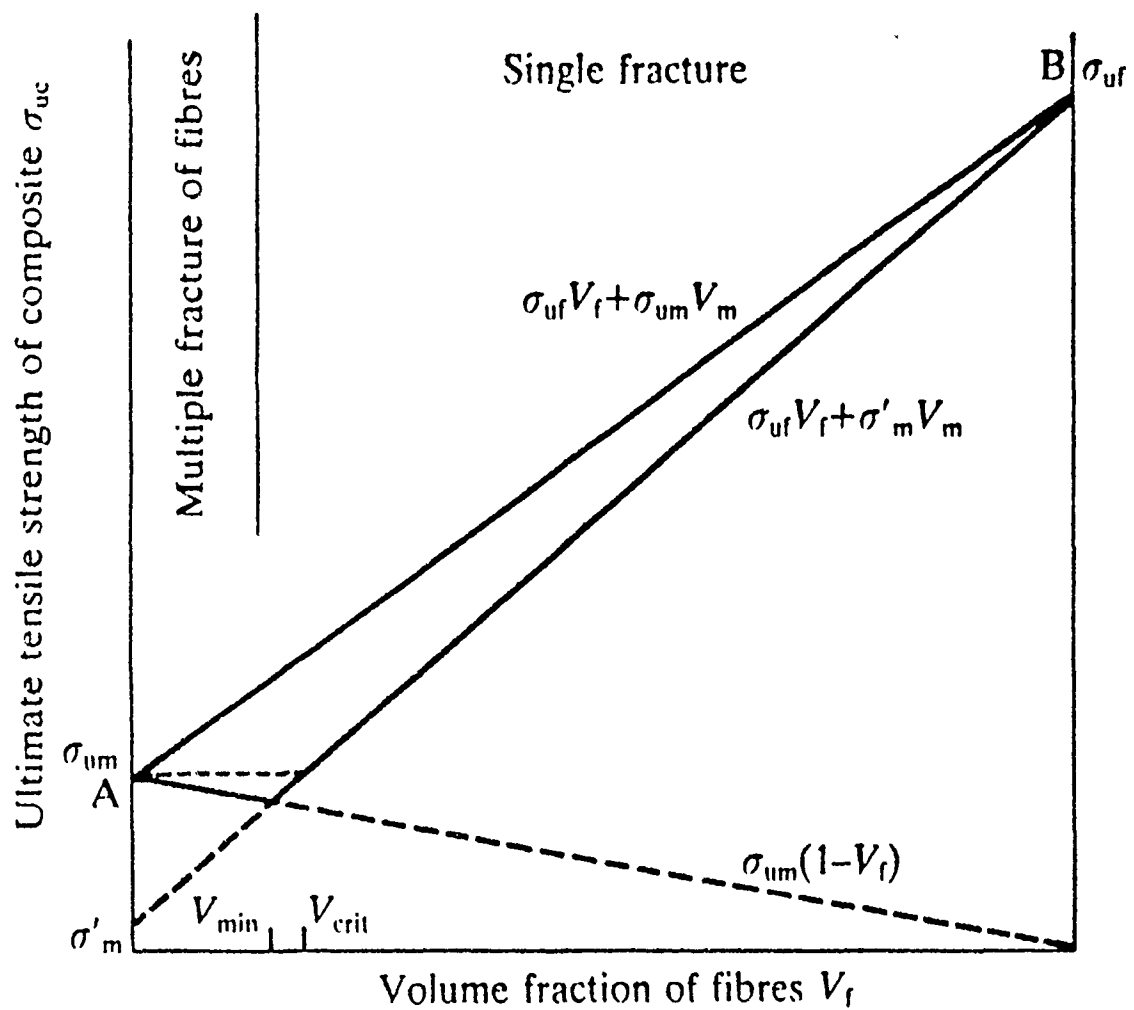
Figure 4.1. The envelope of possible strengths for a composite with ductile
and with brittle fibers

the matrix will fail first. In this case there will be a critical value of the volume fraction. The transition point between the matrix or the fiber failing first will occur at a volume fraction of:

$$V_f = \sigma_{um}/(\sigma_{um} + (\sigma_{uf} - \sigma'_f)) \qquad\qquad 4.14$$

where σ'_f is the stress on the fibers at the point of failure strain of the matrix. For volume fractions smaller than that given by 4.14 the matrix will fail first. For larger volume fractions, the composite will crack into a series of thin discs with a thickness between x' and $2x'$. We can determine a value for x' by calculating the stress transfered to the matrix by the fibers because of the shear force at the interface sufficient to break the matrix. If $d\sigma$ is the stress transferred to the matrix in the distance dx, then:

$$V_m d\sigma = (2V_f/r)\tau dx \qquad\qquad 4.15$$

since $2V_f/r$ is the area of interface per unit length of the composite so that the shear force is given by $(2V_f/r)\beta dx$. Therefore, in order to transfer a stress equal to the maximum, σ_{um}, we have that:

$$x' = (V_m/V_f)(\Sigma_{um}r/2\tau) \qquad\qquad 4.16$$

After cracking is complete, the slope of the stress-strain curve will equal $E_f V_f$ until failure at a stress of $\sigma_{uf}V_f$. The predicted composite strength as a function of fiber fraction is shown in Figure 4.2. It should be noted that the work done in the cracking process depends only on the elastic modulus of the
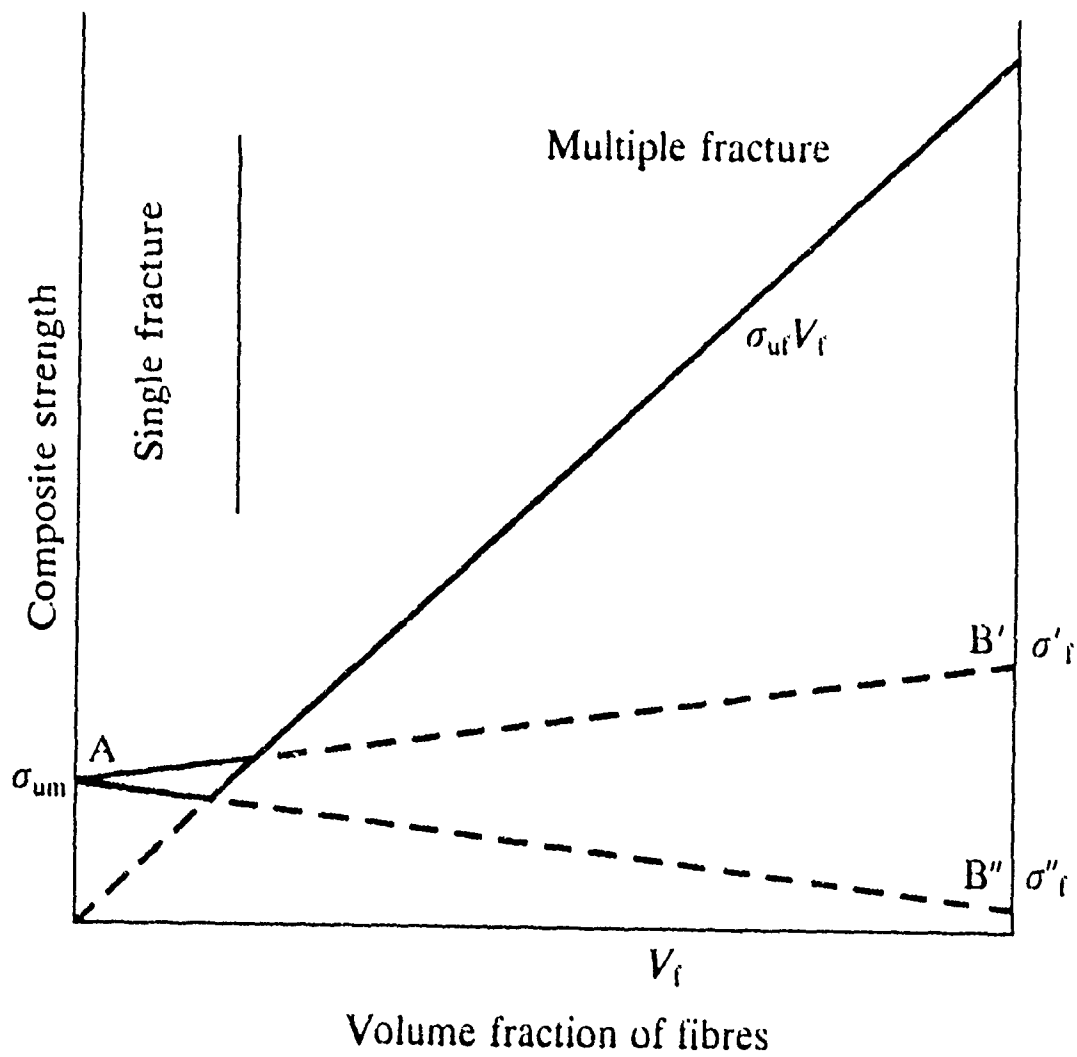
Figure 4.2. Predicted variation of the composite strength as a function of the fiber fraction for strong fibers

composite and the cracking strain of the matrix. The area of cracked surface produced in a unit volume is proportional to V_m/x' and therefore to $2V_f/r$. If we assume that the production of a unit area of crack surface requires an energy of g_m then the work necessary to produce the cracks is proportional to $g_m V_f/r$ and therefore can be made to increase without limit by decreasing the fiber radius. This will require infinite energy as the fiber diameter goes to zero and so the matrix can be made to resist cracking, resulting in extremely large failure strains. This is of particular interest to us in this project as this concept can be used to significantly increase the strength of high temperature ceramics using aligned fibers.

For metallic matrices, stress is transferred to the fibers by plastic flow. Metals have some advantages over ceramics in that they can decrease the notch-sensitivity of the composite, they have high thermal conductivities, low thermal expansion coefficients, and are stable over long times and over wide temperature variations. One of the problems of incorporating fibers of oxides such as sapphire in a metal matrix is that these oxides possess lower surface energies than most metals. Because of this the equilibrium contact angle between the molten metal and the solid oxide is steep. Therefore, fibers of these oxides are not easily incorporated into the molten metal. This problem can be overcome by coating the fibers with a high melting point metal by vacuum deposition or sputtering. Also, infiltration of the fibers can be aided by controlling the atmosphere during incorporation and by using additives.[43] However, it should be pointed out that carbides and borides have lower contact angles than the oxides so that they should be more easily incorporated into metals. Of course, the metals are of considerable interest because of the wide variety of ways that the material can be fabricated into a composite structure as well as by casting the molten metal around the fibers. Powder metallurgical methods can be used, where the fibers and a metal powder are pressed and

sintered in the same way as with ceramic composites. A metal composite can also be produced by electrodeposition, by electroless deposition, and by spraying. These methods have been reviewed by Chou, Kelly, and Okura.[44]
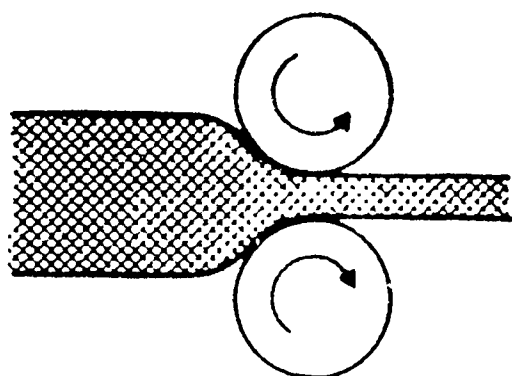
LASER HEATED PEDESTAL GROWTH TECHNIQUE

It is clear from the discussion given earlier that the growth of crystal fibers of high melting point materials must overcome several difficult challenges in order to be useful for the many applications listed. A number of techniques have been used to produce single crystal fibers and these are schematically illustrated in Figure 5.1.

In the hot rolling process, shown in Figure 1 (a), a rod is extruded through a series of progressively smaller wire dies to produce a fiber of reduced diameter.[45] The method is primarily applicable to relatively soft materials with low melting points, e.g. alkali halides.

In the capillary-Bridgeman approach, Figure 1(b), a glass capillary tube is immersed in a melt of the crystal to be grown. The apparatus is slowly lowered through a temperature gradient to produce a crystalline core inside the glass tube.[46] Capillary-Bridgeman growth has primarily been applied to low-melting point organic crystals, as thermal expansion matching and chemical compatibility are critical requirements in this technique.

A number of techniques, for example the edge-defined film-fed growth and related processes, involve feeding the melt through a capillary to a die, which serves to shape the resulting fiber[47], Figure 1(c). These methods are reviewed in reference 48 Single crystal fibers of silver and thallium halides have been produced by such techniques[49,50], as have lower quality fibers of high melting point oxides such as sapphire, lithium niobate and spinel [47] Particularly for high melting point materials, the choice of appropriate die material is crucial to minimize contamination of the melt and provide proper wetting conditions for stable growth. For sapphire growth with such a high melting point, this technique leads to in-diffusion of
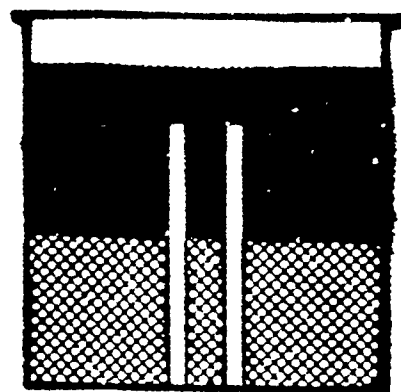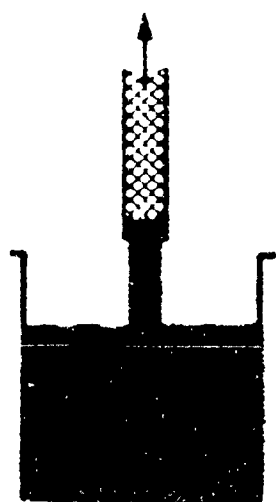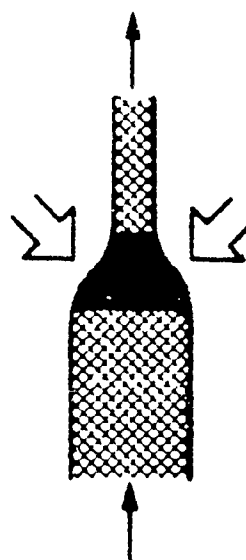
Figure 5.1. Techniques for the growth of single crystal fibers. (a) hot rolling;
(b) Bridgeman growth in glass capillaries; (c) edge-defined film-fed
growth; (d) laser-heated pedestal-growth (LHPG)

33

the die metal such as molybdenum.

Laser-heated pedestal growth (LHPG), illustrated in Figure 1(d), uses a focussed laser beam to melt the tip of a solid rod of the material to be grown. A seed crystal is dipped into the melt, then withdrawn at a faster rate than the source rod is fed in, resulting in the growth of a fiber of reduced diameter. This approach has the advantages of eliminating any possibility of crucible contamination and of achieving melt temperatures limited only by the available laser power. Moreover, difficulties in the stabilization of the fiber diameter have in large part been solved. LHPG has been applied primarily to refractory oxide materials[8,10,51], though halides, borides, and elemental semiconductors have also been grown.[52]

No one of these approaches is best suited to the production of high quality fibers in all materials. We have focused on the refractory oxide materials, for which LHPG offers great flexibility and has the potential to produce the purest fibers.

As mentioned earlier, the LHPG technique involves melting the tip of a source rod with a focussed laser beam, dipping in an oriented seed crystal, then pulling a fiber while feeding in the source rod. This process, quite simple in principle, has several attractive features from a materials processing standpoint.

(1) Very high temperatures can be achieved, limited in principle only by the radiation temperature of the laser, and in practice by the available laser power. Only a few watts of absorbed laser power are necessary to raise the temperature of 500 μm diameter rods of typical oxide materials to their melting point.

(2) The temperature gradients at the freezing interface are on the order of thousands of degrees per cm. These large temperature gradients, in turn, allow stable growth at rates orders of magnitude larger than in bulk crystals, typically 0 1-20mm/min. As thermal stresses in a surface cooled cylinder

34

scale with the radius, these large gradients do not lead to a cracking problem in small diameter fibers.

(3) The process is entirely crucibleless, minimizing the incorporation of undesired dopants, and facilitating the growth of a variety of materials in the same apparatus with a high degree of purity equal to the purity of the starting material.

(4) It is theoretically predicted that in the absence of phase separation or volatilization, the composition of the source rod and the fiber should be identical, so that the effective distribution coefficient approaches unity[52-54], which is particularly important in the growth of compositionally uniform solid-solution crystals. The prediction that convection in the molten zone is not oscillatory further reduces the probability of compositionr' striations.

In order to take advantage of these features of the LHPG process to produce fibers of high melting point materials, stable growth conditions must be realized, which in turn requires thermal and mechanical stability of the growth zone, and symmetric heat input from the laser. The heat should be delivered to a spot whose size is comparable to the source rod diameter, to produce the short molten zones necessary for stable growth. The apparatus designed to meet these requirements is now described.

A block diagram of our fiber growth apparatus is shown in Figure 2. A focused CO_2 laser melts a surface tension supported liquid zone which bridges the source and seed rods. Growth proceeds by simultaneous upward translation of the seed and source rods with the molten zone positioned between them. The laser focal spot, and consequently the molten zone, remain fixed during fiber growth. The source rod to fiber diameter ratio is set by mass conservation to be the square root of the fiber to source rod translation rate.

In order to achieve a constant fiber diameter, stable fiber growth conditions must be realized. This in turn dictates a rigid mechanical apparatus, smooth source feed and fiber pull rates, stable laser power, and symmetric heat input

35

into the molten zone. The LHPG apparatus utilizes novel optical and mechanical systems to achieve stable growth conditions and a uniform diameter fiber. Descriptions of the fiber growth apparatus sub-systems are given below.

A polarized CO_2 laser serves as the heat source for crystal growth. The water cooled laser cavity is temperature stabilized and produces a polarized HE_{11} output mode with power fluctuations of less than 0.75%. A polarization power control system is used to adjust the laser power incident on the molten zone. After passing through a ZnSe beam expanding telescope and some beam steering optics the CO_2 beam enters the controlled atmosphere growth chamber.

Within the growth chamber a novel optical system focuses the laser beam onto the fiber with a 360 degree axially symmetric distribution as shown in Figure 3. The symmetric irradiance prevents cold spots in the growth zone and represents a significant improvement over the previously used two beam,[55] rotating periscope,[56] or ellipsoidal[57] focusing systems.

A novel optical element incorporated into the design is a reflexicon[58] which consists of an inner cone surrounded by a larger coaxial cone. In order to achieve good optical performance it is critical that the reflexicon's two cones be accurately aligned. A mated surface design using diamond turned copper optical components, assures centering of the cone's axes. A gold coating on the copper optical surfaces enhances reflectivity and protects the copper substrate. The reflexicon and parabolic mirror provide near diffraction limited f/2 focusing, yielding a minimum spot size of 30 microns. This tight focus is important for the stable growth of small diameter fibers. The focal spot size can be controlled by modifying the input beam divergence with the focusing telescope X-Y stages on the fiber and source rod translation devices permit adjustment of the fiber position with respect to the fixed laser focal spot.
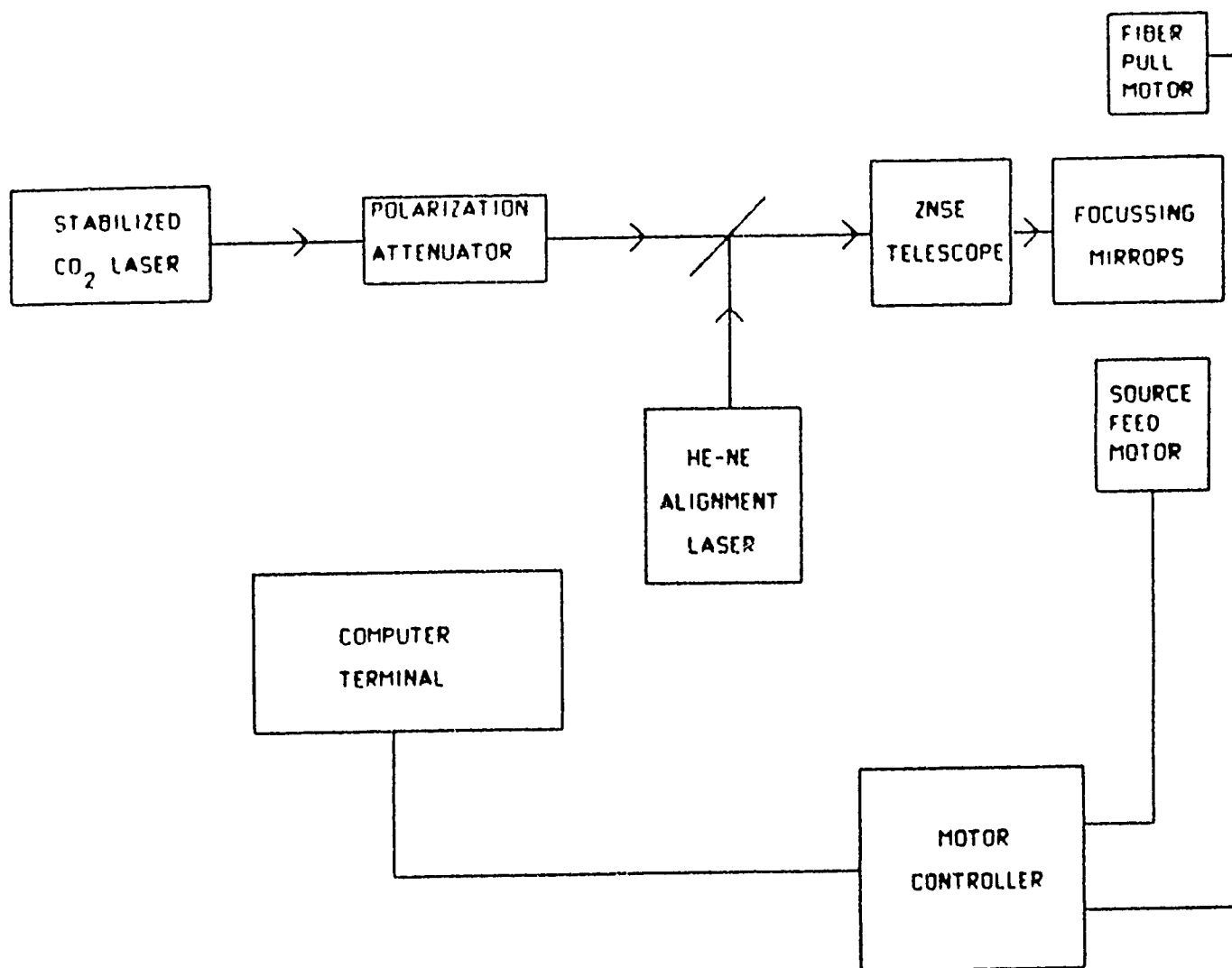
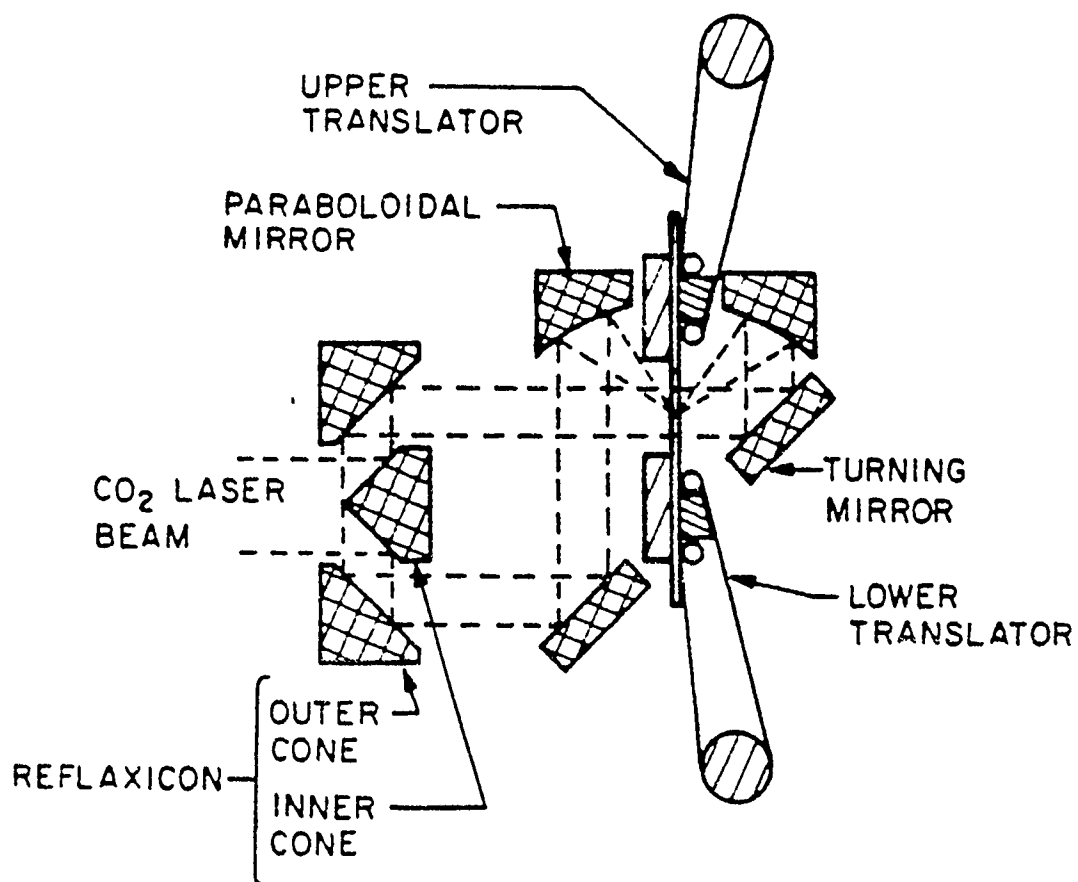Figure 5.2. Block diagram of the LHPG apparatus.

Figure 5.3. Cross-section of the growth head, showing the reflexicon focussing system and the fiber translation mechanisms. The optical elements are rotationally symmetric about their centerline.

Fiber translation speed is controlled by a phase-locked control circuit which enables d.c. motor operation over a 250,000:1 speed range with acquisition times of 1 ms. A useful control option allows the pull-to-feed translation ratio to be fixed while adjusting the growth speed. Since starting transients exist during initiation of fiber growth, a slow growth rate allows time for adjustments. As the equilibrium growth conditions are reached, the growth speed can be increased without affecting the fiber diameter.

The first step in the growth of a fiber is the preparation of the source material. The requirements on the source rod are: (1) it should have the composition of the desired end product (assuming that no volatilization takes place during growth); (2) it should have constant density, and have as close to theoretical density as possible; (3) the cross-section should be constant, as small as possible, and preferably circular. We have had good success using a centerless grinder to fabricate starting rods with diameters as small as 300 μm and tapers as small as 1 μm/cm. The rod material itself can be a single crystal obtained elsewhere, a polycrystalline source material from solidified melts, a cold-pressed and sintered powder, or a hot-pressed powder. All of these have been used successfully.[11,59,60]

The next step in the growth is to melt the tip of the source rod with the CO_2 laser beam, and to dip in a seed crystal. The seed can be an oriented centerless-ground rod, a previously grown fiber or, in the case of a first growth, a platinum wire or a fiber of a higher melting point material. Because of the symmetrical heat input of the reflexicon focussing system, the azimuthal orientation of the seed has no direct effect on the growth.

After the seed is oriented, the laser power is adjusted to produce the desired length of molten zone. The molten zone must also be adjusted to produce the proper contact angle between the melt and the seed.

Growth is initiated at this point by simply simultaneously switching on the pull and feed motors, which have previously been set to run at the appropriate

39

speeds. Lengths over 100 cm have been grown to date. In principle, lengths of fiber are limited only by the available feed material. This latter limitation is not serious in practice, in that each centimeter length of 1.25 mm diameter feed material could produce 5 meters of 50 μm diameter fiber if processed three times.

Only a modest amount of power is necessary to produce an appropriate molten zone. For example, 2 watts incident power is adequate for the growth of a 170μm diameter sapphire fiber from a 500μm diameter source rod. Typical growth rates are 0.1-20 mm/min, several orders of magnitude faster than is typical of bulk crystal growth. The mechanism that limits the maximum possible growth rate appears to vary for different materials. In Reference 603, Nightingale shows that for sapphire grown at rates faster than 8 mm/min, constitutional supercooling with respect to an unknown species, possibly Al or O_2 leads to the formation of microvoids along the axis of the fiber that cause severe optical scattering problems. Growth in a He atmosphere to increase the thermal gradients at the interface may lead to higher useful growth rates.

We have generally found it possible to grow fibers approximately a factor of three smaller in diameter than the source rod for growth in air. As the diameter reduction is increased, the damping coefficient for diameter variation decreases, eventually becoming negative at a critical diameter reduction R_c. Growth at diameter reductions larger than R_c is thus unstable. For Al_2O_3 this instability occurs at a reduction between 3 and 4 when grown in air. It is possible that diameter reductions between 4 and 5 could be achieved when grown in a helium atmosphere.

LaserGenics Corporation has recently obtained the exclusive rights to the three patents held by Stanford University on this single crystal fiber growth process using the LHPG technique. We are developing this process in order to

40

obtain high quality single crystal fibers of several meter lengths. The LHPG technique is an excellent method to grow single crystal fibers. It is likely that for many high melting point materials no other technique will be able to grow similarly good quality single crystal fibers.

With this process, the atmosphere can be accurately controlled during growth as well as the crystal growth temperature. Because of the steep thermal gradients in the growth zone with this technique, the crystal structure that is "frozen in" can to some degree be controlled. We feel that this is an ideal technique to investigate the growth of high melting point materials. This technique is closely related to the float-zone method which is the best known technique to grow incongruently melting compositions.

Section 6

RESULTS AND CONCLUSIONS

Single crystals of TiC and TiB$_2$ are not commercially available so that we were unable to obtain these as source material for our program. We purchased four inch wafers two millimeters thick of both TiC and TiB$_2$. The wafers were formed by hot pressing fine powders of the pure materials. These were subsequently cut into ?mmx2mm square bars. The bars were ground on a centerless grinder to 800μm in diameter. These served as the source material. Initially a platinum wire served as the nucleation point for the fiber growth. After preliminary fibers were grown, these served as seed fibers for later growth runs. Both the TiC and TiB$_2$ were difficult to melt with source rods of this diameter. The TiB$_2$ seemed to have a tendency to sublime in an air atmosphere. We were only able to grow relatively short lengths of this material in air. Growth in an inert atmosphere (Argon) proved superior to an oxidizing atmosphere. The growth temperature had to be controlled quite accurately as stable growth could not be achieved with a relatively small variation in the melt temperature. It was also necessary to grow these two materials at a slow rate. The growth rate for stable growth was at or less than 1mm/minute. It is possible that the rate can be increased with a different atmosphere or with a purer atmosphere than we were able to achieve.

With the source material that we had available, we grew fibers that had a diameter of around 250μm. Smaller diameters could be grown by using the initial fibers as source material but we did not have sufficient time to make many attempts at fiber diameter reduction.

Fibers of several centimeters were grown. Microscopic investigation of these fibers indicated that the fibers were polycrystaline. This is probably due

to the fact that the CO_2 laser was not adequately stabilized. For high melting point materials, it is necessary to reduce the temperature fluctuations as much as possible. We had recently installed a new laser that was specified to have a stability of better than 0.75%. This is the most stable commercial laser on the market at this time. It was discovered later, however, that problems in the pumping system resulted in amplitude variations that were outside the specifications of the laser. We feel that this fact explains the polycrystaline nature of the fibers grown and of the limited lengths achieved.

A tensile tester was used to determine the strength of these fibers even though we did not expect strengths near what we had anticipated because of the polycrystal nature of the fibers. The tensile tester is shown in Figure 6.1 The fibers were mounted in epoxy and then tested by pulling in the tester until the elastic limit was exceeded. These tests resulted in a maximum tensile strength of approximately 1.7 GPa. Earlier tests of sapphire yielded strengths appreciably greater than this. Clearly, in order to improve on these results we must improve the crystal quality.

In order to increase the fiber lengths, we must utilize the process demonstrated on a program with the National Science Foundation. With this process the length of the fiber is limited only by the amount of source material available.
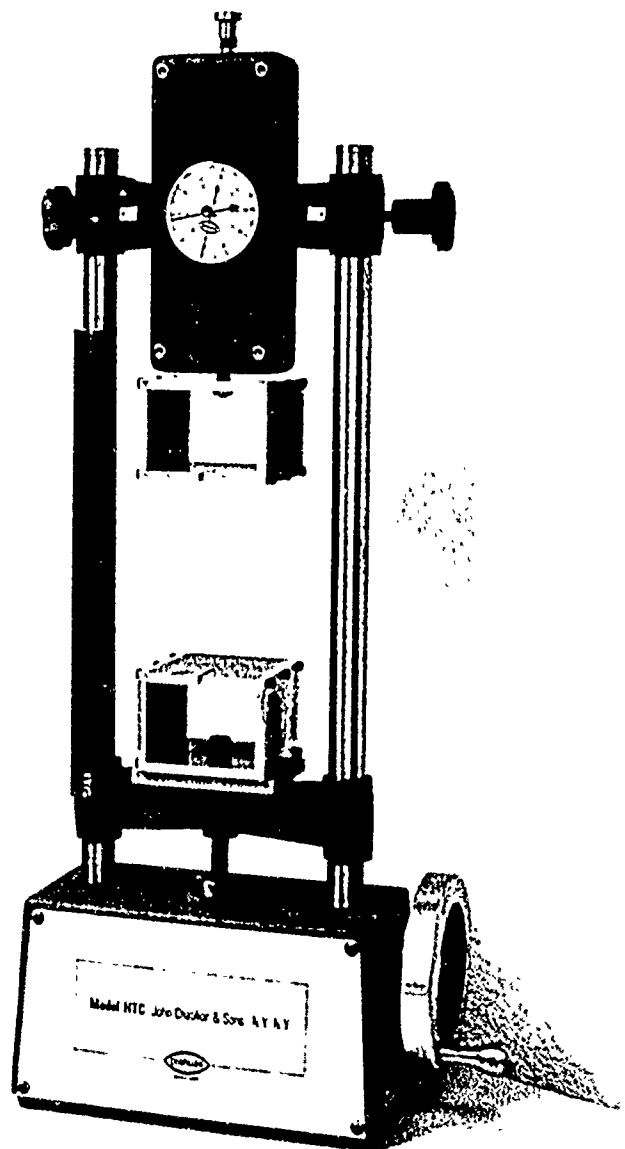
Figure 6.1 Tensile tester

REFERENCES

1. Brenner, S. S., J. Metals 14, 809 (1962)

2. von Gomperz, E., Z. Phys. 8, 184 (1922)

3. Gaule, G. K. & Pastore, J. R., <u>Metallurgy of Elemental and Compound</u> <u>Semiconductors</u> (Interscience Publishers, New York, 1960) p. 201

4. LaBelle, H. E. & Mlavsky, A. I., Nature 216, 574 (1967)

5. Wachtman, J. B. & Maxwell, L. H., J. Amer. Ceram. Soc. 42, 432 (1959)

6. Reed, T. B. & Fahey, R. E., Rev. Sci. Instr. 37, 59 (1966)

7. LaBelle, H. E. & Mlavsky, A. I., Mater. Res. Bull. 6, 571 (1971)

8. Haggerty, J. S., Final Report NASA-CR-120948 (May,1972)

9. Gasson, D. G. & Cockayne, B., J. Mater. Sci. 5, 100 (1970)

10. Burris, C. A. & Stone, J., Appl. Phys. Lett. 26, 318 (1975)

11. Stone, J. & Burris, C. A., J. Appl. Phys. 49, 2281 (1978)

12. M. Polyani, Z. Phys. 7, 323 (1921)

13. E. Orowan, Rep. Prog. Phys. 12, 185 (1949)

14. J. H. de Boar, Trans. Faraday Soc. 32, 10 (1936)

15. F. Zwicky, Phys. Z. 24, 131 (1923)

16. N. H. Macmillan, in <u>Atomistics of Fracture</u>, (eds. R. M. Latanision and J. R. Pickens) pg. 95, Plenum Press, New York (1983)

17. N. H. Macmillan & A. Kelly, Proc. R. Soc. A330, 291 (1972)

18. J. Frenkel, Z. Phys. 37, 572 (1926)

19. J. K. Mackenzie, Ph. D. Thesis, Bristol University (1949)

20. W. R. Tyson, Phil. Mag. 14, 925 (1966)

21. N. H. Macmillan, Ph. D. Thesis, Cambridge University (1969)

22. N. H. Macmillan & A. Kelly, Proc. Roy. Soc. A330, 291 (1972)

23. N. H. Macmillan & A. Kelly, Proc. Roy Soc. A330, 309 (1972)

24. S. Kobayashi, K. Maeda & S. Takeuchi, Acta Metall. 28, 1641 (1980)

25. K. Huang, F. Milstein & J. A. Baldwin, Phys. Rev. B10, 3635 (1974)

26. Z. S. Basinski, M. S. Duesbery & R. Taulor, in "Proc. 2nd Int. Conf. on Metals and Alloys", Americal Society for Metals, Metals Park, Ohio pg. 118

27. K. Nishioka & J. K. Lee, Phil. Mag. A44, 779 (1981)

28. F. Milstein, J. Appl. Phys. 44, 3833 (1973)

29. M. Parinello & A. Rahman, J. Appl. Phys. 52, 7182 (1981)

30. V. L. Gilyarov, Sov. Phys. Solid State 25, 544 (1983)

31. F. C. Frank, Symp. on Plastic Deformation of Crystalline Solids, pg. 89, Carnegie Institute of Technology, Pittsburgh, Pa. (1950)

32. J. P. Hirth, Symp. of the National Physical Laboratory, 15, 218 (1963)

33. J. J. Gilman, Proceed. Symp. on the Physics and Chem. of Ceramics, Ed. by C. Klingsberg, pg. 240, Gordon & Breach, New York (1963)

34. C. E. Inglis, Trans. Institute Naval Archi. 55, 219 (1913)

35. G. Kolosoff, Z. Math. Phyz. 62, 26 (1914)

36. S. Timoshenko & J. N. Goodier, Theory of Elasticity, 2nd Ed. McGraw-Hill, New York (1951)

37. J. Schijve, Analysis of the Fatigue Phenomenon in Aluminum Alloys, Technical Report M2122, N. A. A. R. I., Amsterdam (1964)

38. S. M. Bishop, Stress Near an Elliptical Hole in an Orthotropic Sheet, Technical Report 72026, Royal Aircraft Establishment, Farnborough, England (1972)

39. R. Hill, J. Mech. Phys. Solids 11, 357 (1963)

40. Z. Hashin, J. Mech. Phys. Solids 13, 119 (1965)

41. R. Hill, J. Mech. Phys. Solids 12, 194 and 213 (1964)

42. Z. Hashin, J. Appl. Mech. 50, 481 (1983)

43. A. Kelly and G. J. Davies, Metall. Rev. 10, 1 (1965)

44. T-W Chou, A. Kelly and A. Okura, Composites 16, 187 (1985)

45. R. R. Turk, "Rolling a KCl fiber: a feasibility study", Proc. SPIE 320,

"Advances in infrared Fibers II", 93-101 (1982).

46. B. Nayar, in Technical Digest of the Topical Meeting on integrated and Guided Wave Optics, (O.S.A. Washington D.C., 1982), paper ThA2.

47. H. E. LaBelle, Mat. Res. Bull. 6, 581 (1971).

48. J. Crystal Growth 50(1), (1980) is entirely devoted to shaped crystal growth, and includes a bibliography complete up to that date.

49. Y. Mimura, Y. Okamura, Y Komazawa, and C. Ota, Japanese J. of Appl. Phys. 19, L269 (1980).

50. T. J. Bridges, Optics Lett. 5, 85 (1980).

51. M. Fejer, J. Nightingale, G. Magel and R. L. Byer, Rev. Sci. Instr. 55, 1791 (1984).

52. R. S. Feigelson, "Growth of fiber crystals", Crystal Growth of Electronic Materials, ed. by E. Kaldis, North-Holland, New York, 127-145 (1985).

53. T. Fukuda and H. Hirano, J. Cryst. Growth 35, 127 (1976).

54. S. Matsumura and T. Fukuda, J. Cryst. Growth 34, 350 (1976).

55. J. Stone and C. A. Burrus, Fiber and Integrated Optics 2, 19 (1979).

56. U. C. Paek, Appl. Opt. 13, 1383 (1974).

57. J. E. Midwinter, Optical Fibers for Transmission, John Wiley & Sons, New York, NY, 194 (1979).

58. W. R. Edmonds, Appl. Opt. 12, 1940 (1973).

59. R. S. Feigelson, W. L. Kway and R. K. Route, Proc. SPIE 484, 133 (1984)

60. J. L. Nightingale, "The Growth and Optical Applications of Single-Crystal Fibers", Ph.D. thesis, Stanford University (1985)